Clouds at Arctic Atmospheric Observatories. Part II: Thermodynamic Phase Characteristics

MATTHEW D. SHUPE

Cooperative Institute for Research in Environmental Science, and NOAA/Earth System Research Laboratory, Boulder, Colorado

(Manuscript received 6 January 2010, in final form 1 November 2010)

ABSTRACT

Cloud phase defines many cloud properties and determines the ways in which clouds interact with other aspects of the climate system. The occurrence fraction and characteristics of clouds distinguished by their phase are examined at three Arctic atmospheric observatories. Each observatory has the basic suite of instruments that are necessary to identify cloud phase, namely, cloud radar, depolarization lidar, microwave radiometer, and twice-daily radiosondes. At these observatories, ice clouds are more prevalent than mixed-phase clouds, which are more prevalent than liquid-only clouds. Cloud ice occurs 60%–70% of the time over a typical year, at heights up to 11 km. Liquid water occurs at temperatures above −40°C and is increasingly more likely as temperatures increase. Within the temperature range from −40° to −30°C, liquid water occurs in 3%–5% of the observed cloudiness. Liquid water is found higher in the atmosphere when accompanied by ice; there are few liquid-only clouds above 3 km, although liquid in mixed-phase clouds occurs at heights up to about 7–8 km. Regardless of temperature or height, liquid water occurs 56% of the time at Barrow, Alaska, and at a western Arctic Ocean site, but only 32% of the time at Eureka, Nunavut, Canada. This significant difference in liquid occurrence is due to a relatively dry lower troposphere during summer at Eureka in addition to warmer cloud temperatures with more persistent liquid water layers at the far western locations. The most persistent liquid clouds at these locations occur continuously for more than 70 h in the autumn and more than 30 h in the winter. Ice clouds persist for much longer than do liquid clouds at Eureka and occur more frequently in the winter season, leading to a total cloud occurrence annual cycle that is distinct from the other observatories.

1. Introduction

Cloud thermodynamic phase is a first-order cloud characteristic that shapes the roles that clouds play in the climate system. Due to the molecular properties of water in the liquid and solid phases, and the global distributions and types of aerosol particles, the microphysical properties of liquid and ice clouds differ significantly. Cloud condensation nuclei, upon which cloud liquid droplets form, typically occur in much higher concentrations than ice-forming nuclei, which act as the seeds for cloud ice particles (e.g., Pruppacher and Klett 1997; Rogers and Yau 1989). As a result, cloud liquid droplets occur in higher number concentrations than ice crystals, and consequently are also typically smaller in size.

This fundamental difference between populations of ice and liquid cloud hydrometeors has significant implications on the processes through which clouds interact with the climate system. When considering the radiative effects of clouds, microphysical distinctions between liquid and ice impact the cloud optical depth and other optical properties (Sun and Shine 1994; Gayet et al. 2002). For a fixed amount of condensed mass, the cloud optical depth is highest when the mass is distributed over a larger concentration of smaller particles (Twomey 1977). Thus, liquid clouds have typically been found to more strongly interact with atmospheric radiation than ice clouds (e.g., Sun and Shine 1994; Hogan et al. 2003a; Shupe and Intrieri 2004; McFarquhar and Cober 2004). Cloud phase also defines the microphysical processes that act upon hydrometeor populations. For example, at a given supersaturation, water vapor will more readily condense on ice particles than liquid particles due to the lower saturation vapor pressure of ice relative to liquid (e.g., Rogers and Yau 1989). Additionally, microphysical processes such as collision, coalescence, aggregation, riming, and others are dependent on phase (Pruppacher and Klett 1997). As a result, precipitation efficiency and

Corresponding author address: Matthew D. Shupe, R/PSD3, 325 Broadway, Boulder, CO 80305.
E-mail: matthew.shupe@colorado.edu

DOI: 10.1175/2010JAMC2468.1

type are sensitive to cloud phase (Rogers and Yau 1989; Harrington and Olsson 2001; Zhang and Lohmann 2003). Finally, clouds can respond to changes in aerosol concentrations through a number of phase-dependent aerosol indirect effects (e.g., Lohmann and Feichter 2005).

Despite these numerous ways in which cloud phase is important, and perhaps because of them, models struggle to produce clouds with the correct phase composition. This issue is particularly the case for supercooled conditions (temperature $T < 0$°C), where a broad array of models has difficulty producing and maintaining liquid water at these cold temperatures (e.g., Harrington et al. 1999; Jiang et al. 2000; Morrison et al. 2003; Hogan et al. 2003b; Vaillancourt et al. 2003; Marsham et al. 2006; Tjernstrom et al. 2008). In addition to impacting modeled atmospheric radiation, these phase-related issues can affect the modeled precipitation (Gregory and Morris 1996; Jiang et al. 2000). However, evaluating cloud phase in models has been difficult due to insufficient observational datasets used to develop and test model parameterizations and difficulties with unraveling the effects of compensating model errors. For example, Gregory and Morris (1996) indicated better model radiative closure when liquid water was restricted to only temperatures above −9°C, while observations clearly show that cloud liquid occurs at much colder temperatures (Rauber and Grant 1986; Heymsfield et al. 1991; Intrieri et al. 2002). Since clouds play so many significant roles in the climate system, the cloud phase must be correctly specified in order to correctly simulate the climate (e.g., Sun and Shine 1995; Rotstayn et al. 2000).

Relatively little is known about the annual and vertical distributions of cloud phase in the Arctic because the long polar winter and harsh environment inhibit sufficient measurements in that region. Historically, surface observer records have been used to characterize cloud phase occurrence (Vowinkel and Orvig 1970; Warren et al. 1988). However, surface observations can be difficult, particularly for multilayered cloud scenes or when poor visibility due to darkness and/or blowing snow is a factor (Hahn et al. 1995). Since the late 1990s, remote sensors have been used to examine Arctic cloudiness, providing the possibility to avoid some of the subjective pitfalls experienced by surface observers. Using ground-based remote sensor observations over the Arctic sea ice, Turner et al. (2003) and Shupe et al. (2005) presented some information on the annual frequency of occurrence for different cloud phase types and suggested the frequent occurrence of liquid water layers even in the cold winter. However, longer-term and more widely representative observations are needed at a variety of Arctic locations in order to better understand Arctic cloud phase.

Arctic cloud occurrence fraction and macrophysical properties from six atmospheric observatories have been described in depth in a companion paper (Shupe et al. 2011, hereinafter Part I). This paper builds upon and deepens that analysis by distinguishing many of the cloud occurrence characteristics by phase. This study utilizes observations from three of the Arctic cloud observatories described in the companion paper, namely the Department of Energy's (DOE) North Slope of Alaska site in Barrow, Alaska (Stamnes et al. 1999); the joint National Oceanic and Atmospheric Administration (NOAA)–Canadian Network for the Detection of Atmospheric Change (CANDAC) observatory in Eureka, Nunavut, Canada; and the Surface Heat Budget of the Arctic (SHEBA; Uttal et al. 2002) ice station that was deployed in the Beaufort Sea for 1 yr. Each of these observatories employs at least a cloud radar, depolarization lidar, microwave radiometer, and radiosondes. This instrument suite is not only able to identify the presence of clouds, but also provides sufficient information to identify the cloud thermodynamic phase and its vertical distribution.

As in Part I, the definition of ''cloud'' used here is simply based upon the ability of the suite of stationary, ground-based, zenith-pointing remote sensors to distinguish a cloud signal from clear air. This definition is expanded here to include the thermodynamic phase; namely, a cloud is assigned a given phase depending on the ability of the remote sensors to identify that phase. It must be emphasized that all results here are derived from a zenith-pointing perspective wherein clouds drift overhead. Cloud occurrence fraction, or simply cloud fraction, is the amount of time that clouds are present and detectable above the ground-based sensors.

2. Cloud observations

a. Observatories

Arctic atmospheric observatories utilized in this study are restricted to those that have a sufficient suite of instruments to perform more advanced cloud characterizations, including vertical profiling and phase identification. Thus, only three of the six observatories introduced in Part I have sufficient instrumentation (listed in Table 1). These sites are only found in the western Arctic and it is unknown if they are in any way representative of the Arctic cloudiness found in the eastern Arctic.

The observatory in Barrow is located on the northern coast of Alaska with limited local topographic variability, leading to cloudiness that can be either marine or continental in nature depending upon the large-scale flow. The Eureka observatory is located on the edge of

TABLE 1. Arctic atmospheric observatories. For the fourth column, the date range is for the time period over which the specified suite of cloud-observing instruments was employed to identify cloud phase in this study, which may not be identical to the operation of the site as a whole.

Site Name	Site location	Coordinates	Dates of operation	Instruments
Barrow	North Slope of Alaska	71°19′N, 156°37′W	March 2004–February 2006	MMCR, MPL, radiosondes, MWR
SHEBA	Beaufort and Chukchi Seas in the Western Arctic Ocean	75°–80°N, 143°–167°W	October 1997–October 1998	MMCR, DABUL, radiosondes, MWR
Eureka	Ellesmere Island, Nunavut, Canada	80°00′N, 85°57′W	August 2005–October 2009	MMCR, HSRL, radiosondes, MWR

a fjord in the Canadian archipelago, embedded within a complex system of islands and waterways with highly variant topography and surface types. Finally, the SHEBA project made measurements from a ship-based observatory that drifted with the permanent ice pack in the far western Arctic Ocean for a single year. Together these sites represent a sea-ice-covered Arctic Ocean environment, a coastal site, and a complex terrain site, three categories that characterize much of the western Arctic region. However, since the length of time for each of these datasets is limited, ranging from 1 (SHEBA) to 5 yr (Eureka), and the time periods covered do not always overlap, the data presented here likely does not capture the full natural variability of clouds at these locations.

b. Instruments

The instrument suite at each observatory includes, at minimum, a cloud radar, a depolarization lidar, a microwave radiometer, and twice-daily radiosondes. The use of these instruments to distinguish cloud occurrence from a clear-sky background has been described in Part I. Here, the specific instruments and method used to identify the cloud phase are briefly described. The instruments and their pertinent measurements are summarized in Table 2. All references to height are ''above ground level,'' which for all stations is within a few tens of meters of mean sea level.

Each observatory in this study operates a unique type of depolarization lidar. In Barrow there is a micropulse lidar (MPL; Campbell et al. 2002), in Eureka there is a high-spectral-resolution lidar (HSRL; Eloranta 2005), and at SHEBA there was a depolarization and backscatter unattended lidar (DABUL; Intrieri et al. 2002). Both the lidar backscatter and depolarization ratio contain significant information on the hydrometeor phase. As described in the introduction, populations of cloud liquid droplets typically have a larger backscatter cross section than populations of ice crystals due to size and concentration considerations. Additionally, nonspherical ice crystals have relatively high depolarization ratios, while spherical targets such as liquid water droplets have a minimal depolarization ratio (Sassen 1984; Intrieri et al. 2002). One limitation, however, is that lidar wavelengths are readily attenuated by clouds, with full occultation at an optical depth of 3–5(e.g., Sassen and Cho 1992), preventing higher-altitude observations in optically thicker cloud systems.

Observations of reflectivity, mean Doppler velocity, and Doppler spectrum width from the millimeter cloud radar (MMCR; Moran et al. 1998) contain useful signatures for identifying cloud phase. For example, radar reflectivities higher than about -17 dBZ are characteristic of targets that are larger than cloud liquid droplets (e.g., Frisch et al. 1995), suggesting the presence of precipitation in some form when higher reflectivities are observed. Similarly, large downward velocities, particularly when averaged over time, are again consistent with precipitation-size particles. Finally, while complicated by the broadening effects of turbulence, a broader spectrum width is often associated with multiple phases within

TABLE 2. Instruments, measurements, and pertinent specifications for the datasets used in this study. Here, Δz and Δt are the vertical and temporal resolutions of the input measurements, although all data streams have been interpolated to 1-min time resolution for cloud phase identification.

Instrument	Measurements	Pertinent specifications	Derived parameters
MMCR	Reflectivity, mean Doppler velocity, Doppler spectrum width	Δz = 45–90 m, Δt = 4–10 s	Presence, boundaries, phase
HSRL	Backscatter, depolarization ratio	Δz = 30 m, Δt = 30 s	Presence, boundaries, phase
DABUL	Backscatter, depolarization ratio	Δz = 30 m, Δt = 5 s	Presence, boundaries, phase
MPL	Backscatter, depolarization ratio	Δz = >5 m, Δt = >2 s	Presence, boundaries, phase
MWR	T_B	Δt = 30 s	Phase
Radiosonde	T_{atm}	$\Delta t \sim 12$ h	Phase, temperature

a cloud volume (e.g., Shupe et al. 2004), while narrow widths are more characteristic of single-phase clouds.

Cloud phase characterization is enhanced by two- or five-channel microwave radiometers (MWR; Liljegren 1994) measuring sky brightness temperature between 23 and 31 GHz. These observations are used to estimate the precipitable water vapor (PWV) and total condensed liquid water path (LWP). The phase classification is constrained by these retrievals by requiring liquid water to be identified somewhere in the vertical column when the LWP is greater than the retrieval uncertainty of 25 g m^{-2} (Westwater et al. 2001). Radiosonde measurements of atmospheric temperature and moisture profiles are also used in cloud-type classification and for cloud temperature statistics. Basic thresholds at −40°C, the approximate homogeneous freezing temperature, and 0°C, the melting point of water, support the classification method. For phase classification purposes, radiosonde profiles are linearly interpreted in time to provide full temporal coverage. However, for all results relating these sounding measurements to cloud properties, clouds are only considered within 1 h of a temperature sounding under the assumption that temperature changes are insignificant over this time period. Radiosonde relative humidities in the troposphere are likely biased high by up to 3.5% in the winter and low by up to 5% in the summer (e.g., Miloshevich et al. 2009).

c. *Cloud phase classification*

The multisensor, fixed-threshold cloud phase classification of Shupe (2007) is applied to 1-min-interpolated observations from the MMCR, lidar, MWR, and radiosondes. Phase-specific signatures from this collection of instruments are used to distinguish each cloud pixel as ice, snow, liquid, drizzle, liquid cloud plus drizzle, rain, or mixed phase. The definition of each of these categories is based on the ability of the remote sensors to distinguish each phase type within a given volume or cloud layer. A liquid classification, for example, is defined as a cloud layer that is composed entirely of condensed liquid water droplets observable by at least one of the sensors and no sensor is able to detect ice water or some form of precipitation. For complete details on the specific thresholds used for each measurement, please refer to Shupe (2007). The distinctions between cloud and precipitation are based on radar reflectivity and mean Doppler velocity thresholds. Since the distinction between ''ice'' and ''snow'' is arbitrary, these two classes have been combined and are jointly referred to as ice in this analysis. Likewise, ''rain'' and ''drizzle'' have been combined as liquid-phase precipitation and are referred to as rain.

Mixed-phase cloud ''volumes,'' according to the Shupe (2007) classification method, are time–height pixels within which the remote sensors identify both condensed liquid and ice water. A modified definition of mixed-phase cloud is used here, which includes those circumstances when cloud ice is identified directly and continuously below cloud liquid or mixed-phase regions such that the cloud ice forms from and/or interacts with the liquid-water-containing layer. This mixed-phase definition is similar to the Shupe et al. (2006) definition, which states that mixed-phase cloud systems are those that contain liquid and ice water that are associated through microphysical processes within the same contiguous layer but must not necessarily contain both condensed phases in all cloud volumes. The reason for this mixed-phase definition is to distinguish cloud ice that is formed in a uniformly frozen environment from that which is formed in a mixed-phase environment. Finally, a ''mixed column'' indicates the presence of both solid and liquid phases within the vertical column but not necessarily associated with the same contiguous cloud layer or system.

The uncertainty of the classification algorithm is difficult to ascertain since a definitive validation dataset is lacking. Sources of potential error include the temporal interpolation of 12-h soundings, the 25 g m^{-2} uncertainty associated with the LWP retrieval, and the thresholds employed in the classification algorithm. The first of these only affects those clouds that are close to important temperature thresholds at −40° and 0°C, although it is common for other instruments to constrain the retrieval at these times. LWP uncertainty is perhaps the most significant in that clouds with very little liquid water might be falsely classified as ice, or those with no liquid water might be falsely classified as being liquid or of mixed phase. Fortunately, other measurements, such as the lidar depolarization ratio, can identify cloud liquid water quite robustly. Finally, the classification thresholds were largely based on relationships from the literature (see Shupe 2007). Consequentially, classifications for SHEBA and Barrow made using this method result in statistics that are very similar to those from a manual, multisensor cloud-phase classification used in the Shupe et al. (2006) study.

An example of the phase classification, and the modified mixed-phase definition, is given in Fig. 1. Figures 1a, 1b, 1c, and 1e show key input parameters to the classification method, while the classification mask itself is given in Fig. 1d. Radar and lidar measurements clearly indicate a stratiform cloud layer just above 2 km, which begins to precipitate more strongly over the course of the 12-h case. Low lidar depolarization ratios at the top of this layer suggest a continuous liquid water layer; a characterization that is corroborated by the microwave-radiometer-derived LWP. Larger values of radar reflectivity, increased lidar depolarization, and increased radar mean Doppler velocities all consistently support

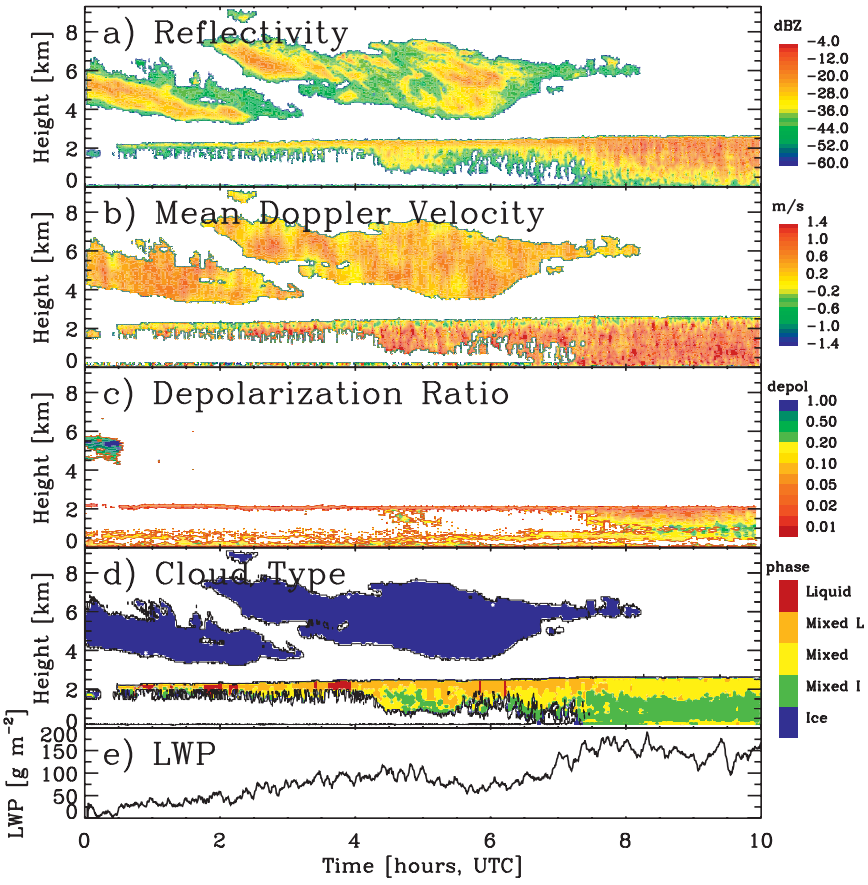

FIG. 1. Example of the cloud phase classification from 21 Sep 2008 at Eureka. (a) Radar reflectivity, (b) radar mean Doppler velocity, (c) lidar depolarization ratio, and (e) microwave radiometer-derived LWP are used as input into the classification algorithm. (d) The classification mask shows areas of ice, liquid, and mixed-phase conditions. Orange and green regions have been modified to account for the definition of mixed-phase cloud used here. All heights are AGL. Mean Doppler velocities are positive downward.

the presence of ice crystals falling from this stratiform liquid layer. An upper cloud layer is also present for the first 8 h of this case, although signal attenuation prevents the lidar from observing this cloud for all but the first 0.5 h (Fig. 1c). During this brief window, the lidar depolarization ratio in this upper cloud indicates ice crystals. The structure of the radar reflectivity supports this classification. Within the classification mask (Fig. 1d), areas that are colored orange and green are those that have been reclassified as mixed-phase cloud from single-phase liquid and ice classifications, respectively. Thus, it is only during brief periods within the first 4 h of the case, when there is no indication of ice crystals forming in and falling from the layer at 2 km, that the layer is classified as containing liquid water only. During all other times, liquid and ice are both detected either within the same volume or vertically adjacent to each other; thus, the layer is classified as mixed phase. A mixed column is present for the whole case except for the brief window in the first 0.5 h when only ice is present in the vertical column.

3. Results

a. Cloud occurrence by phase

Annual cycles of monthly averaged cloud occurrence fraction for different cloud types are summarized in Fig. 2. At each site, the total cloud fraction (black curve) characterizes the subset of observations used in this cloud phase analysis (see Table 1); while these results are similar to the total cloud fractions given in Fig. 2 of Part I, they differ by up to 5%–10% per month due to the specific subset of time periods included in this dataset. To broadly summarize, clouds of any type occur most frequently in the late summer and fall at Barrow

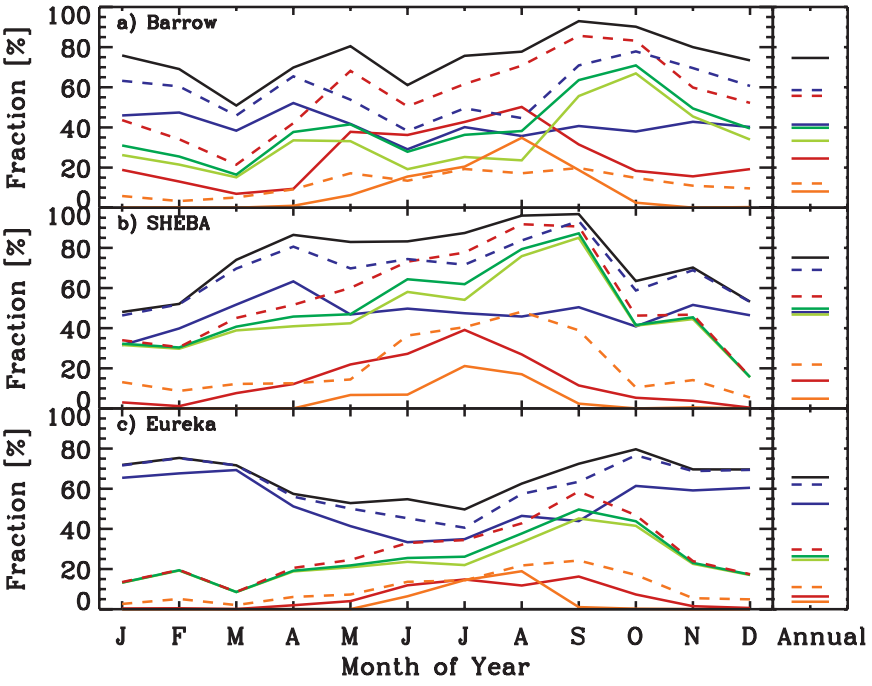

FIG. 2. Annual cycles of monthly mean occurrence fraction for different cloud phase types at (a) Barrow, (b) SHEBA, and (c) Eureka. Curves include the total cloud fraction (solid black), ice-only cloud fraction including snow (solid blue), liquid-only cloud fraction (solid red), liquid precipitation including drizzle and rain (solid orange), mixed-phase cloud fraction (solid light green), and mixed-phase column fraction (solid dark green). See text for definitions of mixed-phase cloud and column. Also included are the occurrence fractions of ice in any type of cloud (dashed blue), liquid in any type of cloud (dashed red), and multiple, distinct layers of liquid water in any type of cloud (dashed orange). Annual average occurrence fractions for each phase type are given at the right.

and during SHEBA, with winter or early spring minima at these sites. Clouds over Eureka are least frequent in the late spring and summer, and occur most often in the winter (see Part I for a more detailed discussion).

Cloud layers composed solely of ice-phase hydrometeors (solid blue curves) occur at annual averages of 41% and 47% of the time at Barrow and SHEBA, respectively. At these two sites, the monthly averages of ice cloud occurrence are typically within ±15% of the annual means, with no clear annual cycle trends but distinct annual maxima in April at both sites. At Eureka, the ice cloud fraction strongly influences the annual variability of total cloudiness and leads to its significant differences from the other two sites. Specifically, Eureka ice clouds occur least frequently in the summer months and most frequently (>65%) in the winter months. The annual average ice cloud fraction of 52% at Eureka is higher than at the other two stations.

The liquid-water-only cloud fraction (solid red curves) tends to follow the annual evolution of the atmospheric temperature and moisture, reaching a summer maximum. However, each site has some distinctive features. Liquid-only clouds occur less than 10% of the time in Eureka and are largely confined to the summer and fall months. During SHEBA, liquid-water-only clouds occurred more often, but were infrequent in winter. All-liquid clouds are present at Barrow nearly one-quarter of the time, with winter occurrence fractions of 10%–20%. Liquid precipitation (solid orange curves) occurs from May through October at Barrow, from May through September during SHEBA, and from June through September at Eureka. Rain and/or drizzle occur about 7% of the time annually at Barrow, but less than 5% of the time at the other sites.

Mixed-phase clouds (light green curves) follow a similar annual cycle at all three sites. They are at a minimum in the winter and early spring months and increase in frequency through the spring and summer months to a maximum occurrence fraction during September or October. Mixed-phase clouds are least frequent in Eureka (25% annual average) and were most frequent during SHEBA (47%). Barrow shows mixed-phase cloudiness maxima in the spring and fall transition seasons, while this feature is less pronounced at the other sites.

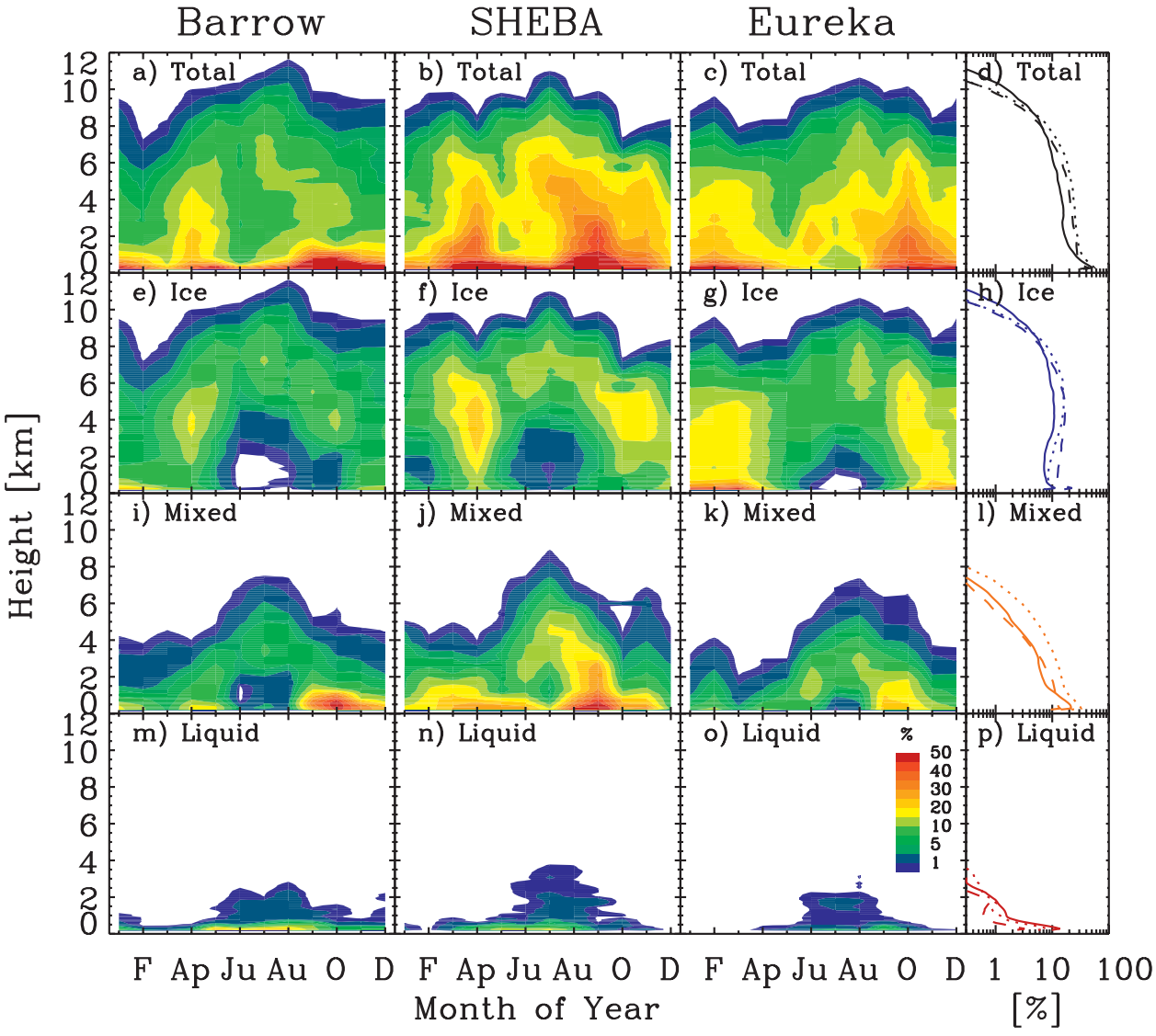

FIG. 3. Vertical distribution of cloudiness distinguished by phase for the three observatories. Contour plots show the mean occurrence fraction of (a)–(c) all cloud, (e)–(g) ice cloud, (i)–(k) mixed-phase cloud, or (m)–(o) liquid cloud as a function of month and height. The first column is for Barrow, the second is for SHEBA, and the third is for Eureka. (d),(h),(l),(p) The annual average profiles of the given cloud phase categories for Barrow (solid), SHEBA (dotted), and Eureka (dashed).

Mixed columns (dark green curves) occur 3%–10% more often than mixed-phase clouds, a difference that is composed primarily of cases containing low-level liquid water clouds and upper-level ice clouds.

When considering the atmospheric column as a whole, it is interesting to examine the occurrence frequency of liquid and ice within any cloud layer, single or mixed phase. At Eureka, the occurrence of cloud ice in the atmospheric column (dashed blue curves) closely follows the annual cycle of ice-only clouds with moderate increases due to the occurrence of mixed-phase clouds. Unlike the other sites, cloud ice at Eureka most often occurs in all-ice clouds, while it occurs as often in mixed-phase clouds only in September. At the other extreme, during SHEBA cloud ice occurs as often or more often in mixed-phase clouds than in single-phase clouds from June through October. At Barrow, this trend occurs only during the fall months. For all sites, cloud ice occurs in the vertical column 60%–70% of the time annually.

Cloud liquid water (dashed red curves), in any cloud layer, occurs most often in the late summer and fall when temperatures are relatively high and moisture is readily available. Liquid water occurs relatively infrequently at Eureka, with an annual occurrence fraction of 30%, a

September maximum, and minimum monthly fractions ranging from 10% to 20%. Liquid water occurs 56% of the time annually at the two far western Arctic locations, and at least ~20% of the time in all months. While liquid water cloud layers occur in similar fractions at both Barrow and during SHEBA, a relatively larger portion of these clouds precipitated ice crystals during SHEBA relative to Barrow.

Finally, multiple, distinct liquid cloud layers (dashed orange curves) occur within the vertical column up to 20% of the time in some summer months, with annual occurrence fractions of about 12% at Barrow and Eureka. While similar during most months, the summer and early fall observations during SHEBA indicated a dramatic increase in multilayered liquid clouds relative to the other sites (as high as 40%), pushing the SHEBA annual occurrence fraction to 22%. These multilayered cloud scenes have been noted as a distinctive Arctic cloudiness phenomenon (e.g., Curry et al. 1996).

b. Vertical distribution

As was discussed in Part I, cloud fraction decreases with increasing altitude at these observatories. However, clouds of different types have unique vertical distributions that vary over the course of the year (Fig. 3). At all sites, the height of the highest ice clouds increases from the winter toward the summer, following the seasonal rise of the tropopause height, and there are few ice clouds below about 2 km in the summer months. At this time, the highest ice cloud fractions are typically at altitudes of 4–10 km. During winter months, particularly at Barrow and Eureka, there is a distinct near-surface maximum in ice cloud occurrence related to thin layers of ice near the surface. These events, often referred to as diamond dust, appear to occur more frequently at the land-based stations relative to the Arctic Ocean site, where diamond dust was observed about 13% of the time from November to May (Intrieri and Shupe 2004). Diamond dust appears to be most prevalent in Eureka.

Mixed-phase clouds mimic the annual evolution of ice clouds, albeit at somewhat lower altitudes. At each site, mixed-phase clouds are most frequent in the lowest 1 km during September and October. Liquid-only clouds typically occur at altitudes less than 2 km and are most common in the summer. By comparing the mixed-phase and liquid-only cloud results, it is clear that liquid water occurs at much higher altitudes when in the presence of cloud ice, and typically does not occur above about 3 km without ice also being present. Liquid water in mixed-phase clouds can exist up to 7–8-km altitude during the summer.

The vertical distribution of cloud phases is summarized in Fig. 4. In the left panels, the relative frequencies of liquid, mixed-phase, and ice clouds are given for each height. On the right in Fig. 4 are the vertical profiles of the total occurrence fractions for liquid and ice phases, regardless of cloud type. These plots reveal the unique quality of the clouds at Eureka relative to the other stations. At Eureka, cloud liquid water is less common and is confined to lower altitudes. Additionally, the near-surface increase in ice cloud occurrence again highlights the frequent diamond dust and low-level ice clouds in Eureka. Thus, even though the vertical distributions of all clouds above Eureka and during SHEBA are quite similar (Fig. 3d and Part I), there are marked differences in the cloud types that compose the vertical distribution. SHEBA and Barrow show many similarities in their

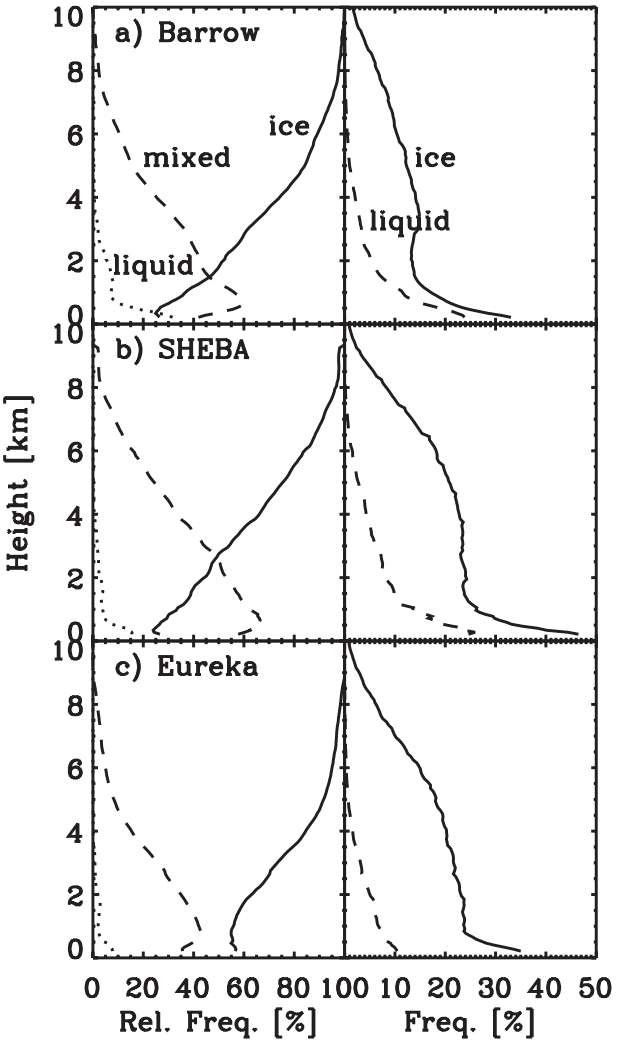

FIG. 4. Annual mean occurrence fraction profiles for (a) Barrow, (b) SHEBA, and (c) Eureka of (left) ice-only, liquid-only, and mixed-phase clouds and (right) liquid and ice in any type cloud. Profiles in the left column have been normalized by the total cloud fraction such that the three curves add up to 100%.

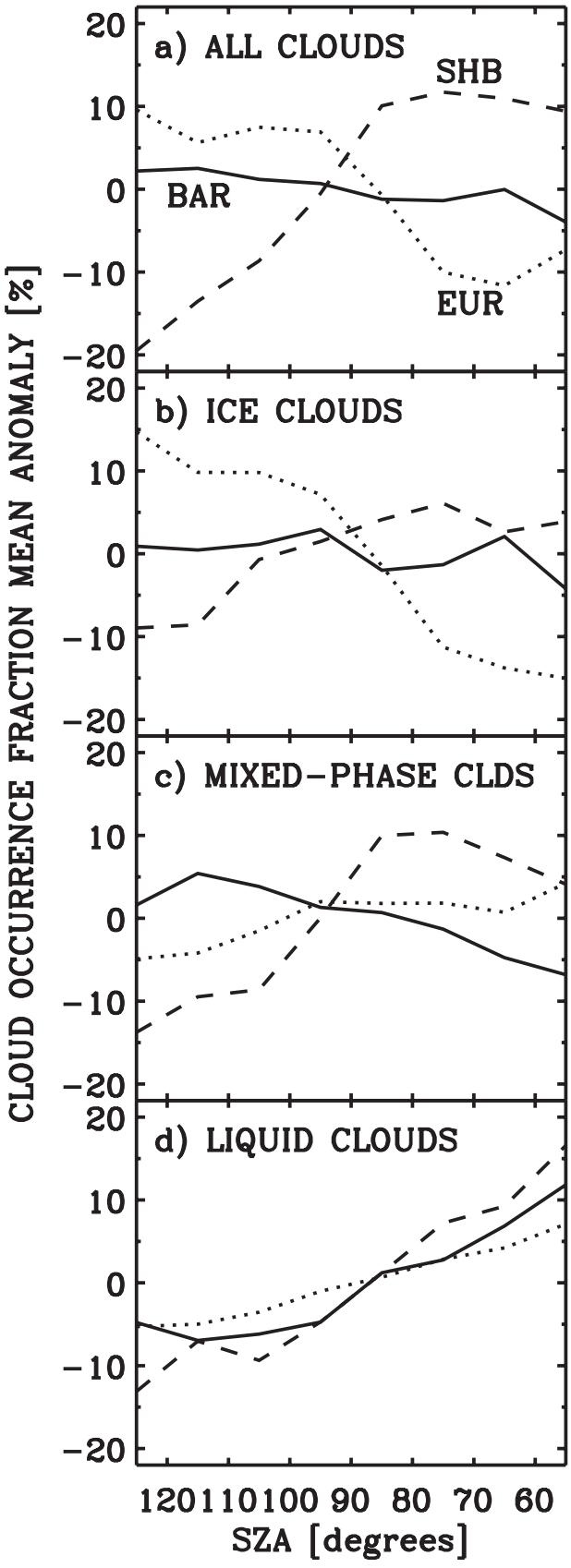

general structure. Important differences between these two sites are primarily centered on the midlevels from 1 to 4 km. In this range, relatively more clouds at Barrow are single-phase liquid or ice, while during SHEBA there were more often mixed-phase clouds.

c. *Diurnal and solar cycles*

Weak diurnal cycles in total cloudiness were identified in Part I, with the strongest diurnal variability being observed during seasons when the sun was above the horizon for at least part of the day. By and large, there is little diurnal variability associated with specific cloud types at these Arctic stations (not shown). A few exceptions should be noted. Diurnal variability in low-level cloudiness during the transition seasons, when the sun is both above and below the horizon within a given day, is driven predominantly by mixed-phase clouds during SHEBA and by both mixed-phase and ice clouds at Eureka. The strongest of these cycles, the mixed-phase clouds during SHEBA, has a diurnal range in occurrence fraction of only 8%. Otherwise, diurnal variability for any cloud type at Barrow or for liquid clouds at any of the sites is typically less than 4%.

An alternate perspective that is related to both the diurnal and seasonal cycles is to examine the relationship between cloud occurrence fraction and solar zenith angle (SZA; Fig. 5). This perspective highlights some of the distinctions among the different observatories that have been suggested in Fig. 2. For total cloudiness, the occurrence fraction does not change much as a function of sun angle at Barrow. During SHEBA, the cloud fraction increased when the sun was above the horizon, while the opposite was true at Eureka (Fig. 5a). In the case of Eureka, the decrease in overall cloudiness with the sun above the horizon is driven by a strong decrease in ice cloud occurrence, in spite of small increases in both liquid and mixed-phase cloud occurrence. The opposite trend of increasing cloudiness during SHEBA when the sun is above the horizon is observed in all cloud types to varying degrees. In Barrow, the apparent insensitivity of cloudiness to sun angle is due to a relative decrease in mixed-phase cloudiness for lower SZA with a commensurate increase in liquid clouds. Therefore,

←

FIG. 5. Mean cloud occurrence fraction anomaly (mean for a given zenith angle minus mean for all zenith angles) as a function of solar zenith angle at Barrow (solid), SHEBA (dashed), and Eureka (dotted) for (a) all clouds, (b) ice clouds, (c) mixed-phase clouds, and (d) liquid clouds. Ten-degree-wide bins are used and each site's latitude determines the relative distribution of data among the different bins.

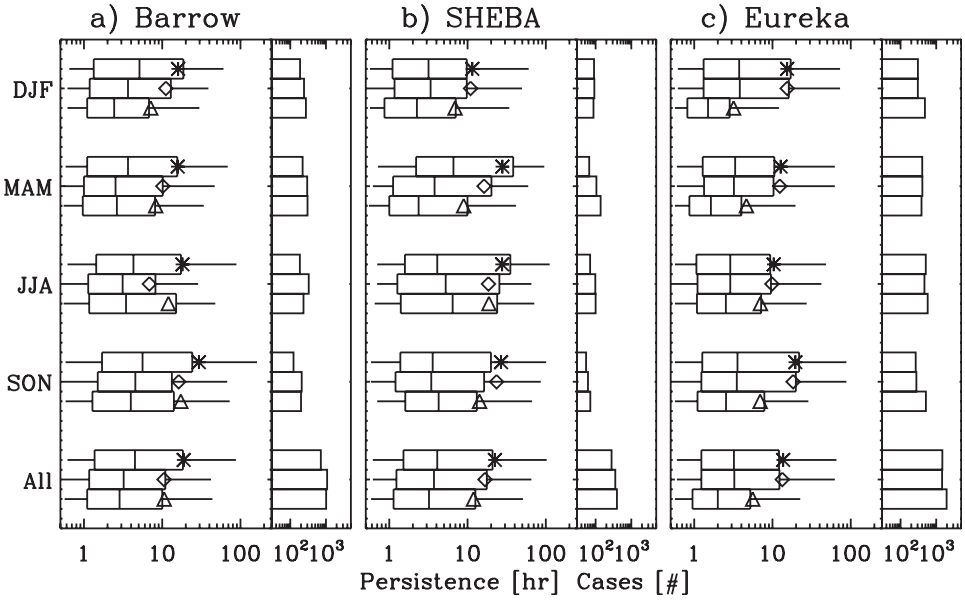

FIG. 6. Cloud-layer persistence statistics by season and cloud phase for (a) Barrow, (b) SHEBA, and (c) Eureka. The persistence is defined as the total time that a cloud is continuously observed by the sensors, neglecting interruptions in cloudiness of less than 0.5 h. A minimum persistence of 0.5 h is required. Each panel provides seasonal and full-year statistics (box-and-whiskers diagrams) for all cloud types (asterisk), ice in any type of cloud (diamond), and liquid in any type of cloud (triangle). Box-and-whiskers diagrams include the median (middle bar), 25th and 75th percentiles (ends of box), 5th and 95th percentiles (end of whiskers), and the mean as a symbol. The number of individual cases contributing to each set of statistics is provided on the right side of each panel.

while liquid clouds at all stations are more frequent when the sun is highest in the sky (i.e., summer), ice and mixed-phase clouds have distinct relationships with the sun angle at the three sites.

d. Cloud persistence

Cloud-layer persistence is directly related to the overall fraction of time that clouds are observed at a given location. Statistics describing the persistence of cloud liquid and ice as a function of season at the three Arctic observatories are presented in Fig. 6. To be included in this analysis, cloudiness must be persistent at some level in the vertical column for at least 30 min, while gaps in cloudiness of less than 30 min are tolerated within longer-lasting clouds. These criteria eliminate intermittent clouds and allow for brief breaks, which may be highly localized, in otherwise continuous cloudiness. Cloud persistence information must be considered within the context of the zenith-viewing perspective of the ground-based remote sensors. First, the statistics simply describe the persistence of cloudiness at any location in the vertical atmospheric column, which often, but not always, describes a single cloud layer. Second, persistence above a given observatory does not necessarily correlate with spatial cloud coverage. Thus, regional differences in topography and synoptic patterns may impact these results.

Cloud-layer persistence statistics are broadly consistent with, and help to explain, many of the results provided in the previous figures. At all stations, cloud liquid water is more persistent during the summer and fall months than at other times of the year, contributing to the overall higher occurrence fractions of liquid-containing clouds in those seasons. Over the full annual cycle at Barrow (Fig. 6a), cloud ice and water tend to persist for similar lengths of time. However, liquid water often persists longer in the summer, while ice persists longer in the winter. During SHEBA (Fig. 6b), ice persisted slightly longer, on average, than liquid water, with similar persistence statistics in summer–fall but ice lasting longer in winter–spring. As has been noted previously, liquid-containing clouds are relatively infrequent in Eureka. At this site, ice perseveres for much longer than cloud liquid in all seasons except summer when the liquid persistence statistics are almost equivalent (Fig. 6c).

Statistics characterizing the most persistent clouds, those above the 95th percentile, tend to support these same general trends and highlight the overall perseverance of Arctic cloudiness. The most persistent 5% of the continuous cloud ice scenes last for longer than about

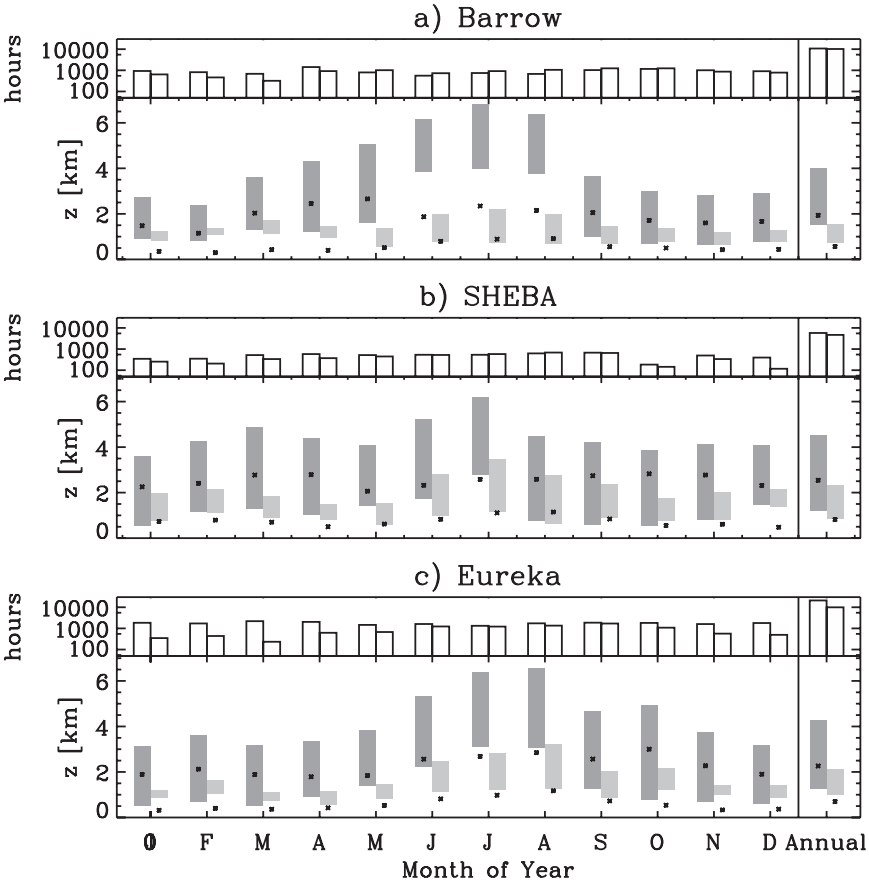

FIG. 7. Monthly mean low base height (bottom of bar), high top height (top of bar), and total thickness (symbol) for cloud ice (dark gray) and cloud liquid (light gray) in any type of cloud at (a) Barrow, (b) SHEBA, and (c) Eureka. Annual mean values are provided on the right side. The total number of hours of 1-min data that contributed to these statistics is provided at the top of each panel.

65 h at Eureka and during SHEBA, but only longer than 42 h at Barrow. For liquid water, 5% of cloud scenes last longer than about 45 h at Barrow and during SHEBA, but only longer than 22 h at Eureka. Looking in more depth at cloud liquid, 5% of cloud liquid scenes persist continuously for at least 70 h in the fall at Barrow and in the fall and summer during SHEBA. Even in the cold winter months, the most persistent liquid water clouds lasts for more than 30 h at Barrow and during SHEBA.

e. Cloud boundaries

Monthly and yearly average statistics on the lowest base height, highest top height, and total thickness of both cloud ice and liquid water are displayed in Fig. 7. Note that the total thickness is often less than the difference between the highest top and lowest base due to multiple cloud layers. At all sites there is a tendency toward thicker liquid water layers in the summer months when both the average lowest liquid base and highest top increase in altitude. Interestingly, there is also a subtle increase in both the average base and top of liquid layers at all sites in February or March. Liquid water vertical boundaries at the three sites are fairly similar when considering annual statistics: average low bases range from 0.75 to 1.0 km, high tops range from 1.5 to 2.3 km, and thicknesses range from 0.6 to 0.8 km. On average, the lowest and thinnest liquid layers are observed at Barrow, while the thickest layers were observed during SHEBA.

Cloud ice layers are, on average, the thickest in spring at Barrow, in summer/fall at Eureka, and in both spring and fall during SHEBA. The highest ice-containing clouds are observed in the summer, and at each site there is an abrupt decrease in highest ice cloud top height in either August or September. Barrow exhibits the most annual variability in monthly mean cloud ice boundaries, ranging from the thinnest and lowest layers in winter to the highest layers in summer. Ice clouds at the three sites are

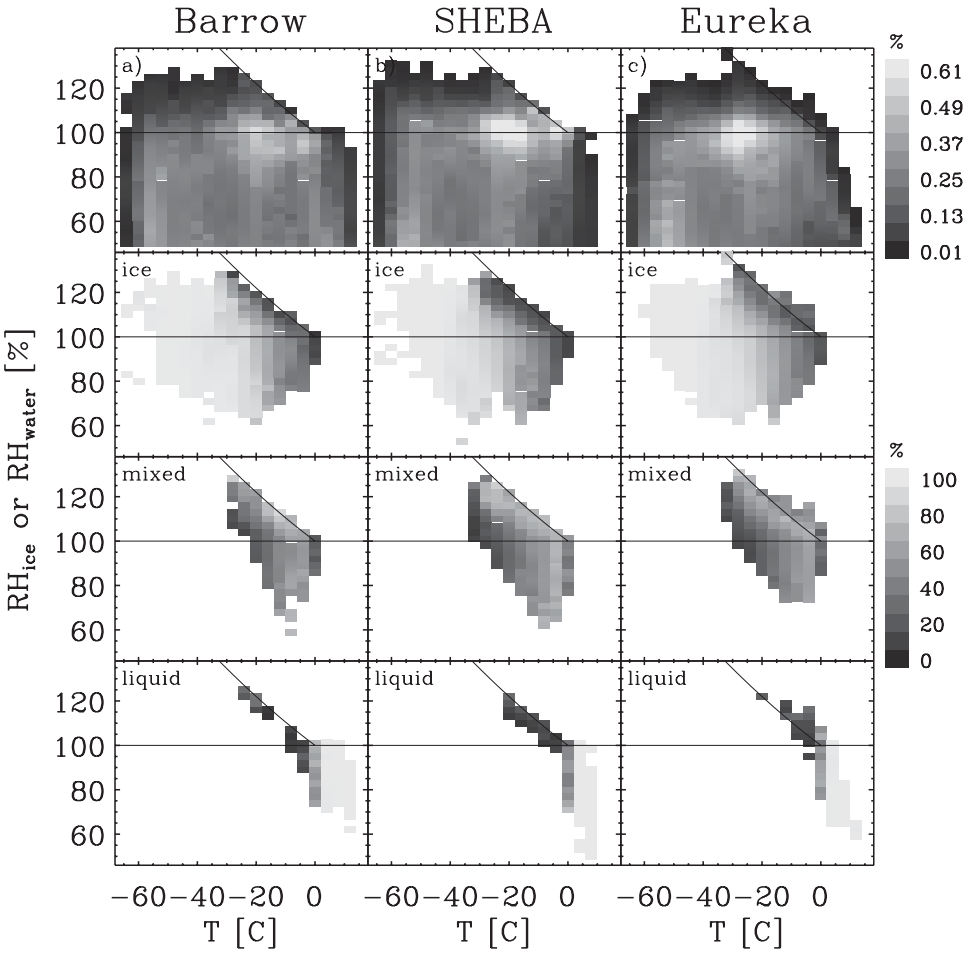

FIG. 8. (top) Two-dimensional histograms of atmospheric temperature and RH for (a) Barrow, (b) SHEBA, and (c) Eureka. These distributions include all of the observations from cloudy and clear-sky conditions that are within 1 h of a radiosonde launch. The RH is determined with respect to ice for temperatures below 0°C and with respect to water for higher temperatures. The lower panels show the relative fractions of in-cloud observations at a given *T*–RH pair that were classified as being ice, mixed phase, or liquid. Here, "ice" includes both cloud ice and snow, while "liquid" includes both liquid cloud and liquid precipitation. In each panel, curves designating saturation with respect to ice and liquid have been provided.

relatively similar on an annual basis, with average low bases ranging from 1.2 to 1.5 km, high tops of 4.0–4.5 km, and thicknesses of 2.0–2.5 km. Again, at Barrow the ice-containing clouds are the thinnest while those during SHEBA were the thickest.

f. Cloud phase as a function of temperature and moisture

The relative occurrence of condensed cloud liquid and ice phases as a function of atmospheric temperature and moisture is a particularly relevant topic for Arctic and global model simulations (e.g., Rotstayn et al. 2000). Moreover, the characteristics and annual evolution of these basic meteorological parameters can explain many of the specific details of cloud phase occurrence observed at these three observatories. Occurrence fractions of the different cloud phase types are given as a function of both temperature and RH, RH alone, and temperature alone in Figs. 8–10, respectively, using radiosonde temperature and RH measurements.

From the perspective of temperature and RH together, there is remarkable consistency in the conditions under which the different cloud types exist (bottom three rows in Fig. 8). Supercooled, all-liquid clouds occur near water saturation over a range of temperatures, while mixed-phase cloud parcels are most common near water saturation but also occur at subsaturation with respect to water, particularly in the ice precipitating below the liquid portion of a mixed-phase cloud. While ice clouds are sometimes observed near the water saturation

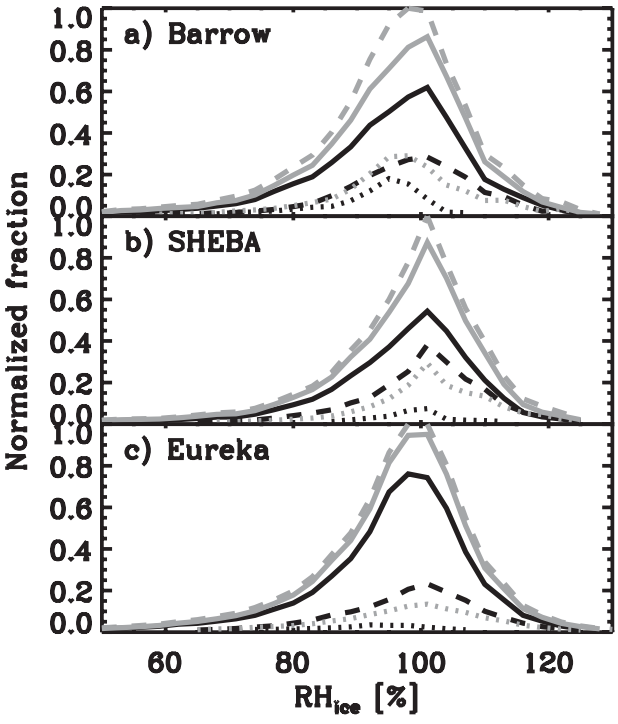

FIG. 9. Distributions of in-cloud RH with respect to ice at (a) Barrow, (b) SHEBA, and (c) Eureka, including all clouds (gray dashed), ice clouds (solid black), mixed-phase clouds (dashed black), liquid clouds (dotted black), ice in any cloud (solid gray), and liquid in any cloud (dotted gray). Here, ice includes both cloud ice and snow, while liquid includes both liquid cloud and liquid precipitation. Three-percent-wide bins are used to construct the distributions, and all curves have been normalized to the peak of the all-cloud distribution for a given site.

curve, they generally occur in conditions that are subsaturated with respect to water. As a result, the annual distributions of cloud type as a function of only RH look very similar among the sites (Fig. 9). There are moderate differences in terms of the total occurrence fractions but only slight differences in terms of the humidity ranges for a given cloud phase type.

Because of the similar patterns of behavior among these sites of cloud phase occurrence as a function of temperature and RH, the differences in total occurrence fractions noted in Figs. 2–6 are therefore due to differences in the overall occurrence fraction of temperature–RH pairs (Figs. 8a–c). Conditions near water saturation that are most favorable for all-liquid and mixed-phase clouds occur less frequently at Eureka compared to the other sites. Particularly during the midsummer, the near-surface RH at Eureka is substantially lower than at the other sites (Part I), leading to the overall low fraction of liquid-containing clouds (Fig. 2) and the minimal low-level cloud fraction (Fig. 3) in those months. Also, relatively colder winter temperatures at Eureka with similar average RHs (Part I and Fig. 8) contribute to the relatively higher winter ice cloud fraction at Eureka in comparison with the other observatories. Finally, the relatively abundant mixed-phase clouds observed at mid- and low levels during SHEBA were a result of the frequent occurrence of atmospheric parcels near or above ice saturation at temperatures between −30° and −10°C relative to the other sites.

Since many models parameterize cloud phase as a function of temperature only, it is also instructive to examine the straight temperature dependence of the phase in these clouds (Fig. 10). It is readily apparent that clouds in Barrow are more frequently observed at warmer temperatures, while those at Eureka are more frequently observed at colder temperatures, relative to the other stations. The most common temperature for cloud occurrence (dashed gray line) is −12°C at Barrow, −20°C during SHEBA, and −28°C at Eureka. These general trends are strongly tied to ice clouds, which are relatively more frequent at warmer temperatures at Barrow and colder temperatures at Eureka.

Cloud liquid water is observed at temperatures as cold as −40°C at each site; however, liquid-water-only clouds are limited to temperatures above about −24°C. Roughly 3%–5% of clouds in the range from −40° to −30°C contain liquid water, while at warmer temperatures there is an increasing probability that clouds will contain liquid. Between −14° and −2°C, mixed-phase clouds are more common than any other cloud type. Only 3%–8% of clouds occur at temperatures above 0°C, and these are nearly all liquid phase. The few cases of mixed-phase clouds at above-freezing temperatures are due either to solid condensate falling into a warm layer, or due to incorrect cloud type classifications, which are probably linked to the temperature interpolation process. When differentiated by cloud height, there is a moderate tendency for liquid water at a given temperature to occur more frequently in clouds below 2 km relative to those above (not shown). This increased likelihood of liquid water is typically on the order of 10%–20% for most temperature ranges at most sites.

Few Arctic-specific aircraft studies exist to compare directly with these results because such datasets are typically periodic in nature and not well suited to creating annually representative statistical characterizations of cloud phase occurrence as a function of temperature. Multiple Arctic and Canadian aircraft cloud observations have been compiled by Korolev et al. (2003) to examine this issue. Relative to that summary, the results presented here show significantly more frequent all-ice clouds at all temperatures, ranging from as much as 40% more at −30°C to ~10% more at −10°C. Similarly, far fewer all-liquid clouds are observed in this dataset at any temperature below 0°C. Finally, mixed-phase clouds at the Arctic observatories are about twice as abundant at

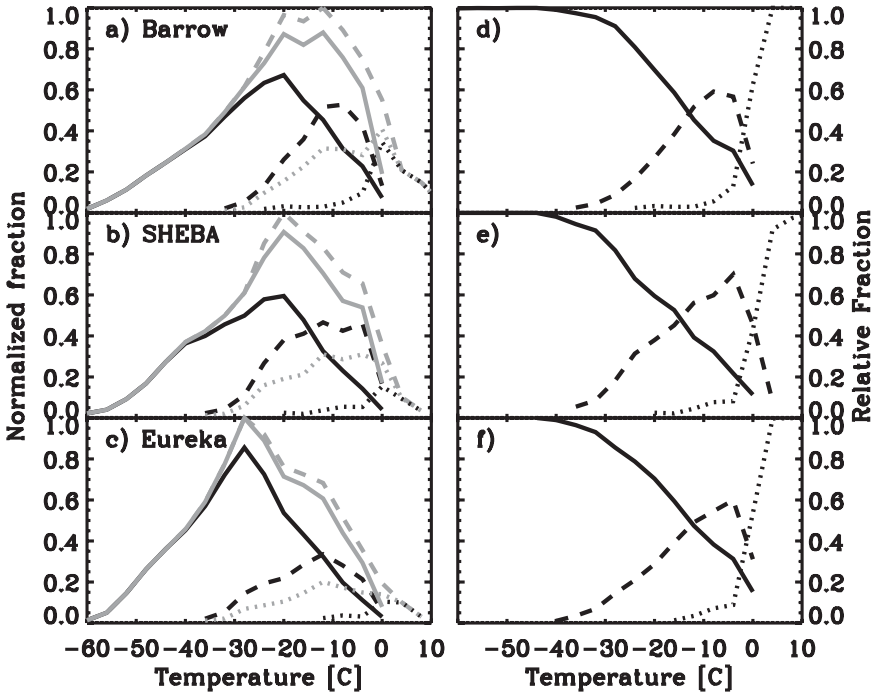

FIG. 10. Distributions of in-cloud temperature at (a),(d) Barrow, (b),(e) SHEBA, and (c),(f) Eureka, including all clouds (gray dashed), ice clouds (solid black), mixed-phase clouds (dashed black), liquid clouds (dotted black), ice in any cloud (solid gray), and liquid in any cloud (dotted gray). As in previous figures, ice includes both cloud ice and snow, while liquid includes both liquid cloud and liquid precipitation. Four-degree-wide bins are used to construct the distributions. (left) Curves have been normalized to the peak of the all-cloud distribution for a given site. (right) All distributions are relative to the total such that they sum to 1.0.

temperatures warmer than −15°C, but less than half as abundant at temperatures below −15°C relative to these aircraft campaigns. For specific aircraft observations, most near the Beaufort Sea area, all-liquid clouds observed by Lawson et al. (2001) were at temperatures very close to 0°C, whereas Hobbs and Rangno (1998) did not observe all-liquid clouds at temperatures lower than −3.5°C in 99 distinct profiles. Arctic mixed-phase clouds have been observed by in situ aircraft over a number of different temperature ranges: from −20° to −8°C (Curry et al. 1990, 1997), from −30° to ~0°C (Hobbs and Rangno 1998), from −26° to −6°C (Pinto 1998; Pinto et al. 2001), from −26° to −3°C (Lawson et al. 2001), from −38° to −4°C (Boudala et al. 2004), from −17° to −3°C (McFarquhar et al. 2007), and as cold as −30°C (Verlinde et al. 2007). Thus, while a direct comparison is not possible, the general results presented here are qualitatively consistent with all of these Arctic-specific observations of cloud phase as a function of temperature.

4. Summary

Arctic cloud thermodynamic phase has been investigated for clouds occurring at three atmospheric observatories in northern Alaska, northern Canada, and the western Arctic Ocean. Each site facility is equipped with a suite of instruments that is sufficient to identify cloud presence, provide vertical profile information, and determine cloud phase. This study builds upon a companion study that examined and compared the total cloud occurrences at these same stations, as well as three others across the Arctic (Part I).

When considering annual-average statistics for the three observatories included in this analysis, ice clouds are more prevalent than mixed-phase clouds, which are themselves more prevalent than liquid clouds. Cloud ice occurs at least 40% of the time during any given month at any observatory, and over the course of a full year it occurs 60%–70% of the time at some height within the vertical atmospheric column. It is observed as high as 11 km, with the highest ice clouds approaching the tropopause height. Ice is observed at temperatures ranging from about −60° to 0°C, and is the only condensed phase observed at temperatures colder than −40°C.

Cloud liquid water is most prevalent and most persistent during the warm summer months, but still occurs at least 10%–20% of the time during winter. It is observed as high as 7–8 km, and is always associated with cloud ice (i.e., mixed-phase cloud) at heights above about

3 km. Liquid water exists at temperatures as cold as −40°C, being present in 3%–5% of clouds with temperatures between −40° and −30°C. Clouds composed entirely of liquid water are observed to occur at temperatures as low as −24°C. At a given temperature, liquid water is more likely to occur in clouds at lower levels than at higher levels. Liquid phase precipitation (rain and drizzle) occurs approximately 5% of the time at these Arctic stations.

In addition to these overarching results, there are significant details that distinguish each of these sites. Broadly, Eureka has the highest fraction of ice clouds, SHEBA has the highest fraction of mixed-phase clouds, and Barrow has the highest fraction of liquid clouds. Cloud liquid water, in any type of cloud, is present 56% of the time at Barrow and during SHEBA, but only 30% of the time at Eureka. These results occur because relatively colder temperatures are observed at Eureka and warmer temperatures are observed at Barrow relative to the other sites, and because the summertime lower troposphere is particularly dry at Eureka. While the total occurrences of liquid water are similar between Barrow and SHEBA, relatively more of these clouds occur as thin, liquid-only clouds at Barrow, while the relatively thicker liquid layers observed during SHEBA more frequently precipitated ice crystals. Consistent with these results, cloud liquid water is more persistent at Barrow and SHEBA, while cloud ice is more persistent at Eureka and SHEBA, when compared to the other sites. The most persistent 5% of liquid water-containing clouds at Barrow and during SHEBA lasted longer than 70 h in the fall and longer than 30 h in the winter. Cloud scenes with multiple liquid layers occurred more often during SHEBA than they do at the other sites, suggesting a possible marine influence on the layering process.

Eureka has a unique annual cycle of total cloudiness relative to the other stations wherein there are relatively fewer clouds in the summer and more clouds in the winter, a cycle that is broadly opposite to those at the other sites. One cause of this cycle is the relatively lower occurrence fraction of liquid-containing clouds in the summer due to the relatively dry lower atmosphere. Eureka's cycle is also driven by the annual variability in ice clouds, which are very frequent in the winter but relatively infrequent in the summer. This winter maximum in ice cloud occurrence is due both to low-level diamond dust and higher-level ice clouds. During all months at Eureka, ice is more likely to occur in ice-only clouds than in mixed-phase clouds. At the other extreme, at SHEBA and Barrow during the summer/fall, ice is more likely to occur in the form of mixed-phase clouds than ice clouds.

These comparative results on cloud phase expand and enhance the cloud occurrence analysis presented in Part I and, thereby, provide insights into observed differences in the cloud occurrence fractions at the different Arctic observatories. It is clear that the annual distributions and variations of cloud phase composition are unique at these three sites, likely driven by regional differences in surface conditions, aerosol properties, topography, and atmospheric circulation. While the broad principles are consistent from site to site, such as the temperature range over which liquid water can occur, these data suggest that models will need to sufficiently incorporate the important regionally varying processes in order to accurately simulate cloud phases at all locations. Moreover, additional studies are required to understand the microphysical and dynamical processes that influence cloud phase on a variety of scales.

While this collection of results provides an important first look at cloud phase derived from ground-based sensors at multiple locations across the Arctic, the observational dataset is relatively sparse. The observations at each existing observatory are limited to a few years at most, which may or may not represent the variability inherent to those sites. Observations over the perennial ice pack of the Arctic Ocean are limited to a single annual cycle, which clearly cannot be representative of a sea ice environment that continues to undergo significant changes (e.g., Comiso et al. 2008; Kay et al. 2008; Perovich et al. 2008). Entirely lacking are cloud observations over the open water of the Arctic Ocean and the landmasses in the eastern Arctic. To understand the spatial and temporal scope of the important cloud properties, a concerted effort is required to expand our Arctic observational capabilities to include more locations and longer observational periods.

Acknowledgments. This research was supported by the National Science Foundation Arctic Observing Network Project (ARC 0632187) and the Office of Science (BER), U.S. Department of Energy (DE-FG02-05ER63965). Observational data used in this study were provided by the Department of Energy's Atmospheric Radiation Measurement Program, the NOAA/Earth System Research Laboratory, and the Canadian Network for the Detection of Arctic Change. Karen Johnson, Connor Flynn, and David Turner are thanked for providing data from Barrow. Ed Eloranta and Taneil Uttal are thanked for providing observations from Eureka.

REFERENCES

Boudala, F. S., G. A. Isaac, S. Cober, and Q. Fu, 2004: Liquid fraction in stratiform mixed-phase clouds from in situ observations. *Quart. J. Roy. Meteor. Soc.,* **130,** 2919–2931.

Campbell, J. R., D. L. Hlavka, E. J. Welton, C. J. Flynn, D. D. Turner, J. D. Spinhirne, V. S. Scott, and I. H. Hwang,

2002: Full-time eye-safe cloud and aerosol lidar observations at Atmospheric Radiation Measurement Program sites: Instruments and data processing. *J. Atmos. Oceanic Technol.,* **19,** 431–442.

Comiso, J. C., C. L. Parkinson, R. Gersten, and L. Stock, 2008: Accelerated decline in the Arctic sea ice cover. *Geophys. Res. Lett.,* **35,** L01703, doi:10.1029/2007GL031972.

Curry, J. A., F. G. Meyer, L. F. Radke, C. A. Brock, and E. E. Ebert, 1990: Occurrence and characteristics of lower tropospheric ice crystals in the Arctic. *Int. J. Climatol.,* **10,** 749–764.

——, W. B. Rossow, D. Randall, and J. L. Schramm, 1996: Overview of Arctic cloud and radiation characteristics. *J. Climate,* **9,** 1731–1764.

——, J. O. Pinto, T. Benner, and M. Tschudi, 1997: Evolution of the cloudy boundary layer during the autumnal freezing of the Beaufort Sea. *J. Geophys. Res.,* **102,** 13 851–13 860.

Eloranta, E. W., 2005: High spectral resolution lidar. *Lidar: Range-Resolved Optical Remote Sensing of the Atmosphere,* K. Weitkamp, Ed., Springer-Verlag 143–163.

Frisch, A. S., C. W. Fairall, and J. B. Snider, 1995: Measurements of stratus cloud and drizzle parameters in ASTEX with a Ka-band Doppler radar and a microwave radiometer. *J. Atmos. Sci.,* **52,** 2788–2799.

Gayet, J.-F., S. Asano, A. Yamazaki, A. Uchiyama, A. Sinyuk, O. Jourdan, and F. Auriol, 2002: Two case studies of winter continental-type water and mixed-phase stratocumuli over the sea. 1. Microphysical and optical properties. *J. Geophys. Res.,* **107,** 4569, doi:10.1029/2001JD001106.

Gregory, D., and D. Morris, 1996: The sensitivity of climate simulations to the specification of mixed phase clouds. *Climate Dyn.,* **12,** 641–651.

Hahn, C. J., S. G. Warren, and J. London, 1995: The effects of moonlight on observation of cloud cover at night and application to cloud climatology. *J. Climate,* **8,** 1429–1446.

Harrington, J. Y., and P. Q. Olsson, 2001: On the potential influence of ice nuclei on surface-forced marine stratocumulus cloud dynamics. *J. Geophys. Res.,* **106,** 27 473–27 484.

——, T. Reisen, W. R. Cotton, and S. M. Kreidenweis, 1999: Cloud resolving simulations of Arctic stratus. Part II: Transition-season clouds. *Atmos. Res.,* **51,** 45–75.

Heymsfield, A. J., L. M. Miloshevich, A. Slingo, K. Sassen, and D. O'C. Starr, 1991: An observational and theoretical study of highly supercooled altocumulus. *J. Atmos. Sci.,* **48,** 923–945.

Hobbs, P. V., and A. L. Rangno, 1998: Microstructures of low and middle-level clouds over the Beaufort Sea. *Quart. J. Roy. Meteor. Soc.,* **124,** 2035–2071.

Hogan, R. J., P. N. Francis, H. Flentje, A. J. Illingworth, M. Quante, and J. Pelon, 2003a: Characteristics of mixed-phase clouds. Part I: Lidar, radar, and aircraft observations from CLARE '98. *Quart. J. Roy. Meteor. Soc.,* **129,** 2089–2116.

——, A. J. Illingworth, E. J. O'Connor, and J. P. V. Poiares Baptista, 2003b: Characteristics of mixed-phase clouds. Part II: A climatology from ground-based lidar. *Quart. J. Roy. Meteor. Soc.,* **129,** 2117–2134.

Intrieri, J. M., and M. D. Shupe, 2004: Characteristics and radiative effects of diamond dust over the western Arctic Ocean region. *J. Climate,* **17,** 2953–2960.

——, ——, T. Uttal, and B. J. McCarty, 2002: An annual cycle of Arctic cloud characteristics observed by radar and lidar at SHEBA. *J. Geophys. Res.,* **107,** 8030, doi:10.1029/2000JC000423.

Jiang, H., W. R. Cotton, J. O. Pinto, J. A. Curry, and M. J. Weissbluth, 2000: Cloud resolving simulations of mixed-phase Arctic stratus observed during BASE: Sensitivity to concentration of ice crystals and large-scale heat and moisture advection. *J. Atmos. Sci.,* **57,** 2105–2117.

Kay, J. E., T. L'Ecuyer, A. Gettelman, G. Stephens, and C. O'Dell, 2008: The contribution of cloud and radiation anomalies to the 2007 Arctic sea ice extent minimum. *Geophys. Res. Lett.,* **35,** L08503, doi:10.1029/2008GL033451.

Korolev, A. V., G. A. Isaac, S. G. Cober, J. W. Strapp, and J. Hallett, 2003: Microphysical characterization of mixed-phase clouds. *Quart. J. Roy. Meteor. Soc.,* **129,** 39–55.

Lawson, R. P., B. A. Baker, C. G. Schmitt, and T. L. Jensen, 2001: An overview of microphysical properties of Arctic clouds observed in May and July 1998 during FIRE ACE. *J. Geophys. Res.,* **106** (D14), 14 989–15 014.

Liljegren, J. C., 1994: Two-channel microwave radiometer for observations of total column precipitable water vapor and cloud liquid water path. Preprints, *Fifth Symp. on Global Change Studies,* Nashville, TN, Amer. Meteor. Soc., 262–269.

Lohmann, U., and J. Feichter, 2005: Global indirect aerosol effects: A review. *Atmos. Chem. Phys.,* **5,** 715–737.

Marsham, J. H., S. Dobbie, and R. J. Hogan, 2006: Evaluation of a large-eddy model simulation of a mixed-phase altocumulus cloud using microwave radiometer, lidar and Doppler radar data. *Quart. J. Roy. Meteor. Soc.,* **132,** 1693–1715.

McFarquhar, G. M., and S. G. Cober, 2004: Single-scattering properties of mixed-phase Arctic clouds at solar wavelengths: Impacts on radiative transfer. *J. Climate,* **17,** 3799–3813.

——, G. Zhang, M. R. Poellot, G. L. Kok, R. McCoy, T. Tooman, A. Fridlind, and A. J. Heymsfield, 2007: Ice properties of single-layer stratocumulus during the Mixed-Phase Arctic Cloud Experiment: 1. Observations. *J. Geophys. Res.,* **111,** D24201, doi:10.1029/2007JD008633.

Miloshevich, L., V. Holger, D. Whiteman, and T. Leblanc, 2009: Accuracy assessment and correction of Vaisala RS92 radiosonde water vapor measurements. *J. Geophys. Res.,* **114,** D11305, doi:10.1029/2008JD011565.

Moran, K. P., B. E. Martner, M. J. Post, R. A. Kropfli, D. C. Welsh, and K. B. Widener, 1998: An unattended cloud-profiling radar for use in climate research. *Bull. Amer. Meteor. Soc.,* **79,** 443–455.

Morrison, H., M. D. Shupe, and J. A. Curry, 2003: Modeling clouds observed at SHEBA using a bulk microphysics parameterization implemented into a single-column model. *J. Geophys. Res.,* **108,** 4255, doi:10.1029/2002JD002229.

Perovich, D. K., J. A. Richter-Menge, K. F. Jones, and B. Light, 2008: Sunlight, water, and ice: Extreme Arctic sea ice melt during the summer of 2007. *Geophys. Res. Lett.,* **35,** L11501, doi:10.1029/2008GL034007.

Pinto, J. O., 1998: Autumnal mixed-phase cloudy boundary layers in the Arctic. *J. Atmos. Sci.,* **55,** 2016–2038.

——, J. A. Curry, and J. M. Intrieri, 2001: Cloud–aerosol interactions during autumn over Beaufort Sea. *J. Geophys. Res.,* **106** (D14), 15 077–15 097.

Pruppacher, H. R., and J. D. Klett, 1997: *Microphysics of Clouds and Precipitation*. Kluwer Academic, 954 pp.

Rauber, R. M., and L. O. Grant, 1986: The characteristics and distribution of cloud water over the mountains of northern Colorado during winter storms. Part II: Spatial distributions and microphysical characteristics. *J. Climate Appl. Meteor.,* **25,** 489–504.

Rogers, R. R., and M. K. Yau, 1989: *A Short Course in Cloud Physics*. Butterworth-Heinemann, 290 pp.

Rotstayn, L. D., B. F. Ryan, and J. J. Katzfey, 2000: A scheme for calculation of the liquid fraction in mixed-phase stratiform clouds in large-scale models. *Mon. Wea. Rev.,* **128,** 1070–1088.

Sassen, K., 1984: Deep orographic cloud structure and composition derived from comprehensive remote sensing measurements. *J. Climate Appl. Meteor.,* **23,** 568–583.

——, and B. S. Cho, 1992: Subvisual-thin cirrus lidar dataset for satellite verification and climatological research. *J. Appl. Meteor.,* **31,** 1275–1285.

Shupe, M. D., 2007: A ground-based multisensory cloud phase classifier. *Geophys. Res. Lett.,* **34,** L22809, doi:10.1029/2007GL031008.

——, and J. M. Intrieri, 2004: Cloud radiative forcing of the Arctic surface: The influence of cloud properties, surface albedo, and solar zenith angle. *J. Climate,* **17,** 616–628.

——, P. Kollias, S. Y. Matrosov, and T. L. Schneider, 2004: Deriving mixed-phase cloud properties from Doppler radar spectra. *J. Atmos. Oceanic Technol.,* **21,** 660–670.

——, T. Uttal, and S. Y. Matrosov, 2005: Arctic cloud microphysics retrievals from surface-based remote sensors at SHEBA. *J. Appl. Meteor.,* **44,** 1544–1562.

——, S. Y. Matrosov, and T. Uttal, 2006: Arctic mixed-phase cloud properties derived from surface-based sensors at SHEBA. *J. Atmos. Sci.,* **63,** 697–711.

——, V. P. Walden, E. Eloranta, T. Uttal, J. R. Campbell, S. M. Starkweather, and M. Shiobara, 2011: Clouds at Arctic atmospheric observatories. Part I: Occurrence and macrophysical properties. *J. Appl. Meteor. Climatol.,* **50,** 626–644.

Stamnes, K., R. G. Ellingson, J. A. Curry, J. E. Walsh, and B. D. Zak, 1999: Review of science issues, deployment strategy, and status for the ARM North Slope of Alaska–Adjacent Arctic Ocean climate research site. *J. Climate,* **12,** 46–63.

Sun, Z., and K. P. Shine, 1994: Studies of the radiative properties of ice and mixed-phase clouds. *Quart. J. Roy. Meteor. Soc.,* **120,** 111–137.

——, and ——, 1995: Parameterization of ice cloud radiative properties and its application to the potential climatic importance of mixed-phase clouds. *J. Climate,* **8,** 1874–1888.

Tjernstrom, M., J. Sedlar, and M. D. Shupe, 2008: How well do regional climate models reproduce radiation and clouds in the Arctic? An evaluation of ARCMIP simulations. *J. Climate Appl. Meteor.,* **47,** 2405–2422.

Turner, D. D., S. A. Ackerman, B. A. Baum, H. E. Revercomb, and P. Yang, 2003: Cloud phase determination using ground-based AERI observations at SHEBA. *J. Appl. Meteor.,* **42,** 701–715.

Twomey, S. A., 1977: The influence of pollution on the shortwave albedo of clouds. *J. Atmos. Sci.,* **34,** 1149–1152.

Uttal, T., and Coauthors, 2002: Surface heat budget of the Arctic Ocean. *Bull. Amer. Meteor. Soc.,* **83,** 255–275.

Vaillancourt, P. A., A. Tremblay, S. G. Cober, and G. A. Isaac, 2003: Comparison of aircraft observations with mixed-phase cloud simulations. *Mon. Wea. Rev.,* **131,** 656–671.

Verlinde, J., and Coauthors, 2007: The Mixed-Phase Arctic Cloud Experiment (M-PACE). *Bull. Amer. Meteor. Soc.,* **88,** 205–220.

Vowinkel, E., and S. Orvig, 1970: The climate of the north polar basin. *Climates of the Polar Regions,* S. Orvig, Ed., World Survey of Climatology, Vol. 14, Elsevier, 129–152.

Warren, S. G., C. J. Hahn, J. London, R. M. Chervin, and R. L. Jenne, 1988: Global distribution of total cloud cover and cloud type amounts over the ocean. NCAR Tech. Note NCAR/TN-317+STR, 212 pp.

Westwater, E. R., Y. Han, M. D. Shupe, and S. Y. Matrosov, 2001: Analysis of integrated cloud liquid and precipitable water vapor retrievals from microwave radiometers during SHEBA. *J. Geophys. Res.,* **106,** 15 099–15 112.

Zhang, J., and U. Lohmann, 2003: Sensitivity of single column model simulations of Arctic springtime clouds to different cloud cover and mixed phase cloud parameterization. *J. Geophys. Res.,* **108,** 4439, doi:10.1029/2002JD003136.